Available online at www.sciencedirect.com
ScienceDirect
Trans. Nonferrous Met. Soc. China 28(2018) 2190−2198
Transactions of Nonferrous Metals Society of China
www.tnmsc.cn

Microstructure and mechanical properties of as-extruded Mg−Sn−Zn−Ca alloy with different extrusion ratios

Yang ZHANG[1], Xiao-yang CHEN[2], Ya-lin LU[1], Xiao-ping LI[1]

1. School of Materials Engineering, Jiangsu University of Technology, Changzhou 213001, China;
2. School of Mechanical Engineering, Jiangsu University of Technology, Changzhou 213001, China

Received 28 August 2017; accepted 22 December 2017

Abstract: The effect of extrusion ratio on microstructure and mechanical properties of as-extruded Mg−6Sn−2Zn−1Ca (TZX621) (mass fraction, %) alloy was investigated. It is found that incomplete dynamic recrystallization (DRX) took place in as-extruded TZX621 alloy. As the extrusion ratio was increased from 6 to 16, both fraction of un-DRXed grains and average size of DRXed grains in as-extruded TZX621 alloy decreased and the basal texture was weakened. Coarse CaMgSn phase was broken into particles and fine Mg_2Sn phase precipitated from α-Mg matrix during hot extrusion. Yield strength, ultimate tensile strength and elongation of as-extruded TZX621 alloy with extrusion ratio of 16 reached 226.9 MPa, 295.6 MPa and 18.1%, which were improved by 36.0%, 17.7% and 13.5%, respectively, compared to those of as-extruded TZX621 alloy with extrusion ratio of 6.

Key words: Mg−Sn alloy; extrusion ratio; microstructure; texture; mechanical properties

1 Introduction

As the lightest structural metallic material, Mg alloys show wide application prospects in the areas of aerospace, automobile and 3C industries due to their potential for weight reduction. However, the relatively poor heat resistance is a main obstacle to the practical application of Mg alloys [1−3]. RE elements are the most effective elements to improve the heat resistance of Mg alloys, but the fancy price of RE elements restricts the large-scale application of Mg-RE alloys [4,5]. In recent years, the development of low-cost heat-resistant Mg alloys has received increasing attention. Due to the high melting point of Mg_2Sn phase (770 °C) and low diffusion rate of Sn element in α-Mg matrix, the heat resistance of Mg−Sn alloys is comparable to Mg−RE alloys [6]. In addition, since Sn element is nontoxic, Al-free Mg−Sn alloys are also promising biomaterials for body implants [7]. Up to now, a lot of studies have been done on Mg−Sn alloys, involving the alloy design, precipitation behavior, plastic deformation, etc.

In order to improve the mechanical properties of binary Mg−Sn alloys, attempts have been made via alloying binary Mg−Sn alloys with different elements. Zn element is a common alloying element in Mg alloys and contributes to solid solution and ageing strengthening simultaneously. In Mg−Sn alloys, the addition of Zn element can refine the distribution of Mg_2Sn precipitates and enhance the age-hardening response. The segregation of Zn atoms at the Mg_2Sn/Mg interface might be responsible for the enhanced nucleation of Mg_2Sn precipitates in Mg−Sn−Zn alloys [8]. The variation of Zn content in Mg−5Sn−xZn (x=1, 2, 4, mass fraction, %) alloys showed little influence on grain size and the basal texture of indirect-extruded samples, and the improvement of comprehensive mechanical properties with the increase of Zn content was attributed to the increased number density of fine Mg_2Sn and MgZn precipitates [9]. Ca element can refine the as-cast microstructure and improve the heat resistance of Mg alloys. In Mg−Sn alloys, the addition of Ca element can lead to the formation of different Ca-contained phases depending on Ca content. The good heat resistance of Mg−4Sn−4Ca (mass fraction, %) alloy was related to the presence of CaMgSn and Mg_2Ca phases which distributed uniformly in the matrix [10].

Plastic deformation, especially extrusion, is often

Foundation item: Project (51601076) supported by the National Natural Science Foundation of China; Projects (16KJB430013, 17KJA430005) supported by the Natural Science Fund for Colleges and Universities in Jiangsu Province, China
Corresponding author: Xiao-yang CHEN; Tel: +86-519-86953210; E-mail: cxy@jsut.edu.cn
DOI: 10.1016/S1003-6326(18)64864-2

used to further refine the microstructure and improve the mechanical properties of Mg−Sn alloys. For example, a Mg−7Sn−1Al−1Zn (mass fraction, %) alloy with high-speed extrudability was developed and the maximum tested speed reached 27 m/min. After extrusion, a completely recrystallized structure consisting of coarse and fine recrystallized grains was obtained [11]. The strength and ductility of Mg−2Sn−1Ca (mass fraction, %) and Mg−2Sn−1Ca−2Zn (mass fraction, %) alloys were improved significantly after hot extrusion [12].

Up to now, the effect of extrusion parameters on the microstructure and mechanical properties of Mg−Sn alloys was rarely investigated. In this work, a new Mg−6Sn−2Zn−1Ca (TZX621, mass fraction, %) alloy was prepared by permanent mold casting and subjected to homogenization. Then, the ingots were hot extruded with extrusion ratio of 6 and 16, respectively. The effect of extrusion ratio on microstructure and mechanical properties of TZX621 alloy was investigated.

2 Experimental

Commercially pure Mg, Sn, Zn (99.9%, mass fraction) and Mg−30Ca (mass fraction, %) master alloy were used to prepare TZX621 alloy in this work. The raw materials were melted in a resistance crucible furnace under the protection of mixed atmosphere of SF_6 (1%, volume fraction) and CO_2 (99%, volume fraction). After the melting of pure Mg, pure Sn, pure Zn and Mg−Ca master alloy were added into the melt at 730 °C and the melt was stirred for 3 min to assure the homogeneous chemical distribution. The melt was held at 730 °C for 10 min before casting and then poured into a permanent mold preheated to 200 °C to prepare cast ingots with dimension of d45 mm × 100 mm. The cast ingots were homogenized with (340 °C, 4 h) + (480 °C, 8 h). A two-stage solution was designed to avoid the possible grain boundary dissolution behavior caused by small amount of Mg−Zn phase with low melting point. The ingots after homogenization treatment were machined into d40 mm × 30 mm for extrusion. The hot extrusion was carried out at 300 °C with extrusion ratio of 6 and 16, respectively, and the extrusion speed of 2 mm/s.

Microstructure specimens of as-cast, homogenized and as-extruded alloys were prepared with standard metallographic procedures, i.e. mechanically ground, polished, and then etched with a mixture of 4.2 g picric acid, 10 mL acetic acid, 80 mL ethyl alcohol and 10 mL water. Phase composition of TZX621 alloy was characterized by XRD (XPERT POWDER). Microstructure characterization was carried out with OM (ZEISS Primotech) and SEM (ZEISS Sigma 500) equipped with EDS. Texture characterization was conducted by EBSD. The specimens for EBSD analysis were initially ground using emery papers from 1200# to 3000#, followed by the pre-polishing using Al_2O_3 suspension (1 and 0.25 mm), and the final polishing using suspension OP-S (0.04 mm-sized SiO_2 particles). Rectangular tensile specimens with gauge length of 15 mm were cut from the extruded bars parallel to the extrusion direction. Tensile test was carried out on an electronic universal testing machine (CMT−5205) with a cross-head speed of 1 mm/min at ambient temperature.

3 Results and discussion

Figure 1 shows XRD patterns of TZX621 alloy in as-cast, homogenized and as-extruded states. As shown in Fig. 1(a), as-cast TZX621 alloy consisted of α-Mg, Mg_2Sn and CaMgSn phases. However, in XRD pattern of TZX621 alloy after homogenization, only the diffraction peaks of α-Mg and CaMgSn phases were observed and the diffraction peaks of Mg_2Sn phase almost disappeared. These results indicated that, during the homogenization treatment, Mg_2Sn phase dissolved into α-Mg matrix while CaMgSn phase with high melting point remained in TZX621 alloy. Figure 1(b) shows XRD patterns of as-extruded TZX621 alloy with

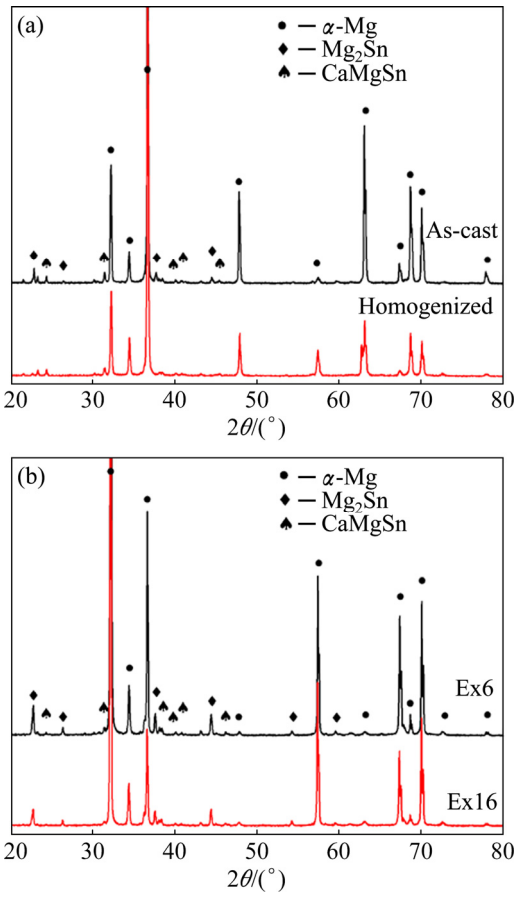

Fig. 1 XRD patterns of TZX621 alloy: (a) As-cast and homogenized; (b) Extrusion ratio of 6 (Ex6) and 16 (Ex16)

extrusion ratio of 6 and 16, respectively. Besides the diffraction peaks of α-Mg and CaMgSn phases, several diffraction peaks of Mg_2Sn phase were found in XRD patterns of as-extruded TZX621 alloy, which indicated that Mg_2Sn phase reformed in TZX621 alloy during hot extrusion.

Figure 2 shows microstructures of TZX621 alloy in as-cast and homogenized states. As shown in Fig. 2(a), coarse α-Mg dendrites and second phases were observed in optical microstructure of as-cast TZX621 alloy. The second phases in as-cast TZX621 alloy presented three different morphologies (seen in Fig. 2(b)). According to EDS results, both the coarse irregularly-shaped phase and the dense fine phase were Mg_2Sn phase, while the coarse needle-like phase was CaMgSn phase. During the solidification of TZX621 alloy, α-Mg dendrites nucleated and grew first. Then, the coarse Mg_2Sn and CaMgSn phases formed at the end of solidification. The morphology of the dense fine Mg_2Sn phase was in line with the morphology features of secondary-precipitated phase [13], which indicates that it was precipitated from supersaturated α-Mg solid solution of TZX621 alloy after solidification. Due to the solute redistribution during solidification, the distribution of Sn element in as-cast α-Mg grains was uneven and Sn atoms aggregated near the grain boundaries. According to Mg−Sn binary phase diagram, the solid solubility of Sn in Mg was 14.85% (mass fraction) at 561 °C and it decreased to only 0.45% (mass fraction) at 200 °C. During the cooling stage after solidification, the solubility of Sn element in Mg reduced greatly, which promoted the precipitation of fine Mg_2Sn phase. Figure 2(c) shows the optical microstructure of TZX621 alloy after homogenization. It is found that, α-Mg grains in TZX621 alloy transferred from dendritic to near-equiaxed. Second phases were still observed inside α-Mg grains and at the grain boundaries. As shown in Fig. 2(d), compared to as-cast TZX621 alloy, the volume fraction of second phases in homogenized TZX621 alloy decreased significantly. Both coarse and fine Mg_2Sn phase disappeared. Coarse needle-like CaMgSn phase remained in homogenized TZX621 alloy, which was in accordance with XRD analysis above.

Figure 3 shows optical microstructures of as-extruded TZX621 alloy with different extrusion ratios. It was found that, dynamic recrystallization (DRX) took place in as-extruded TZX621 alloy during hot extrusion, but DRX process was incomplete. As shown in Fig. 3(a), the as-extruded TZX621 alloy with extrusion ratio of 6 exhibited typical multi-modal microstructure with coarse un-DRXed α-Mg grains elongated along the extrusion direction. According to quantitative metallurgical analysis, un-DRXed region in as-extruded TZX621 alloy with extrusion ratio of 6 was about 31.3%. As shown in Fig. 3(b), the as-extruded TZX621 alloy with extrusion ratio of 16 also presented multi-modal microstructure. Although the extrusion ratio as high as 16 did not lead to the complete DRX process in TZX621 alloy, the change of extrusion ratio showed obvious effect on the fraction of un-DRXed grains. As the extrusion ratio increased from 6 to 16, the fraction of un-DRXed grains decreased from 31.3% to 13.2%. Recrystallization of a certain alloy during hot extrusion was usually influenced by extrusion

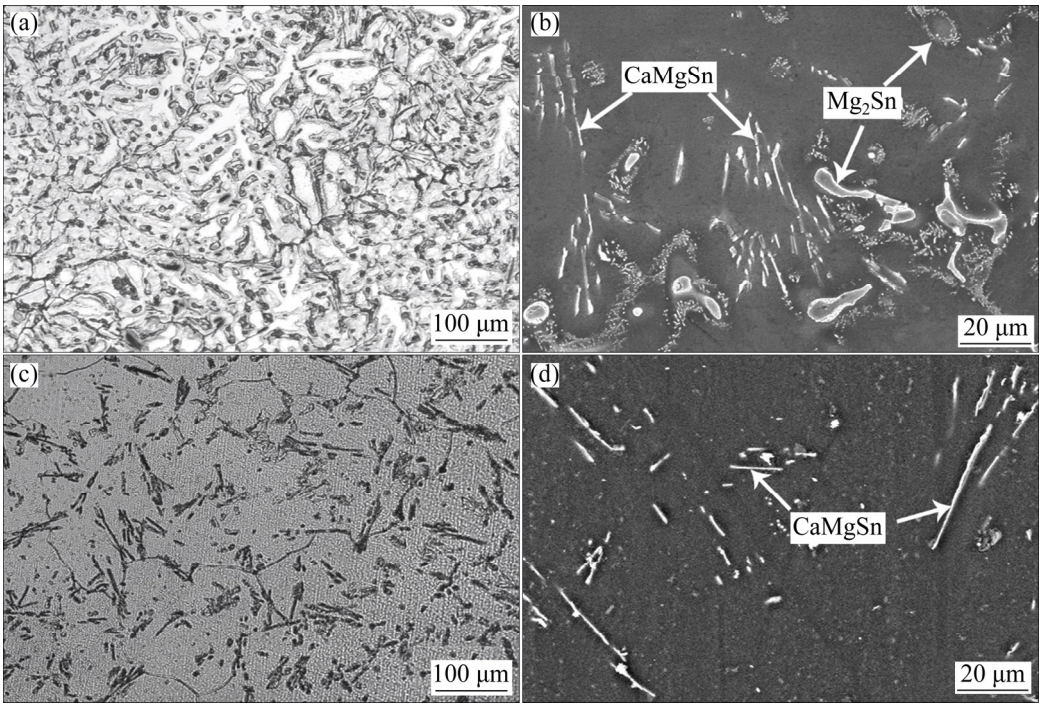

Fig. 2 Microstructures of as-cast (a, b) and homogenized (c, d) TZX621 alloy: (a, c) Optical microstructure; (b, d) SEM image

parameters. In this work, the extrusion temperature was constant (300 °C). Hence, the difference in fraction of un-DRXed grains was mainly due to the change of extrusion ratio. During hot extrusion at the same extrusion speed, a high extrusion ratio could lead to a large total strain, high strain rate, high deformation stress and low recrystallization temperature, which was beneficial to recrystallization [14].

Figure 4 shows microstructures of as-extruded TZX621 alloy with different extrusion ratios observed by SEM. As shown in Figs. 4(a, c), coarse CaMgSn phase remained in homogenized TZX621 alloy was broken into particles and distributed along the extrusion direction. Most of CaMgSn phase was broken into particles with size of about 1 μm, but some coarse particles with size of several micrometers were also observed in as-extruded TZX621 alloy. XRD results of as-extruded TZX621 alloy above proved that, Mg_2Sn phase precipitated during hot extrusion. As shown in Figs. 4(b, d), fine Mg_2Sn particles were observed in as-extruded TZX621 alloy which precipitated from α-Mg matrix due to the thermo-mechanical effect of hot extrusion. The precipitation of fine Mg_2Sn phase during hot extrusion was also observed in the hot-extruded Mg−5Sn−3Zn alloys with Ca addition [15]. Particle stimulated nucleation (PSN) mechanism usually played an important role in recrystallization. Only second particles with size ≥1 μm could promote the dislocation accumulation and lead to the nucleation of new grains [16]. In as-extruded TZX621 alloy, most of the broken CaMgSn particles in as-extruded TZX621 alloy could act as the substrates and therefore promoted the recrystallization. Meanwhile, although the fine Mg_2Sn particles could not act as recrystallization substrates, they had a strong pinning effect to hinder the dislocation movement [17]. Therefore, the precipitation of Mg_2Sn phase also contributed to the

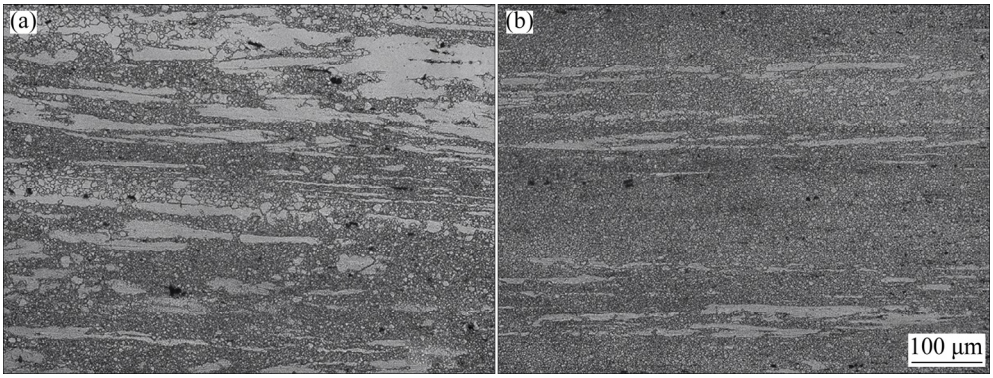

Fig. 3 Optical microstructures of as-extruded TZX621 alloy with different extrusion ratios parallel to extrusion direction: (a) Extrusion ratio of 6; (b) Extrusion ratio of 16

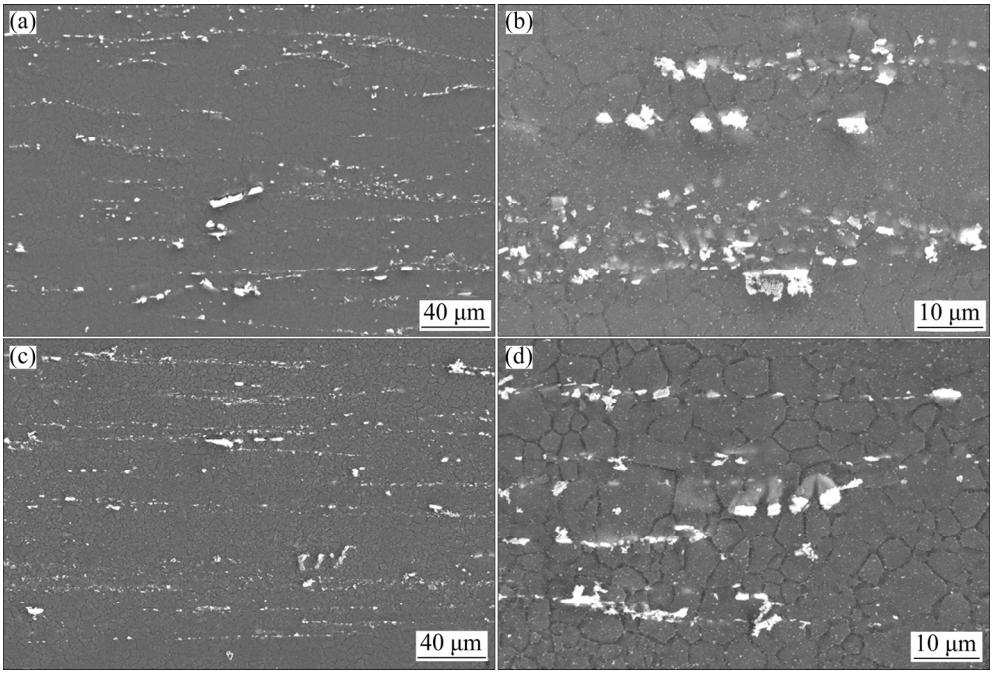

Fig. 4 Microstructures of as-extruded TZX621 alloy with different extrusion ratios parallel to extrusion direction observed by SEM: (a, b) Extrusion ratio of 6; (c, d) Extrusion ratio of 16

grain refinement of TZX621 alloy via restricting the grain growth during hot extrusion.

Figure 5 shows the image mapping results of Mg, Sn, Zn and Ca elements in as-extruded TZX621 alloy with extrusion ratio of 16. As shown in Fig. 5, Sn and Ca elements enriched in certain regions, and the rich regions coincided with broken particles in as-extruded TZX621 alloy, which also confirmed that the broken particles were CaMgSn phase. Furthermore, the distribution of Zn element was relatively uniform, which indicated that Zn element was solid solution element in TZX621 alloy. Although EDS could detect Sn element in the matrix, the enrichment of Sn element due to the formation of fine Mg_2Sn particles was not observed clearly, since the size of precipitated particles was too small.

Figure 6 shows the orientation maps of as-extruded TZX621 alloy with different extrusion ratios obtained by EBSD. The white lines in EBSD orientation maps represented low-angle grain boundaries (LAGBs) with the misorientation angle below 15° and the black lines represented high-angle grain boundaries (HAGBs). As shown in Fig. 6, HAGBs were usually observed in DRXed regions, while LAGBs were often observed inside the un-DRXed grains, which were induced by the dislocation accumulation during hot extrusion. In accordance with optical microstructure, coarse un-DRXed grains were found in as-extruded TZX621 alloy with extrusion ratio of 6. The microstructure of as-extruded TZX621 alloy with extrusion ratio of 6 consisted of coarse un-DRXed, coarse DRXed and fine DRXed grains. In as-extruded TZX621 alloy with extrusion ratio of 16, the fraction of un-DRXed grains was reduced significantly. It is interesting that coarse and fine DRXed grains coexisted in as-extruded TZX621 alloy with extrusion ratio of 6 while the amount of coarse DRXed grains in as-extruded TZX621 alloy with

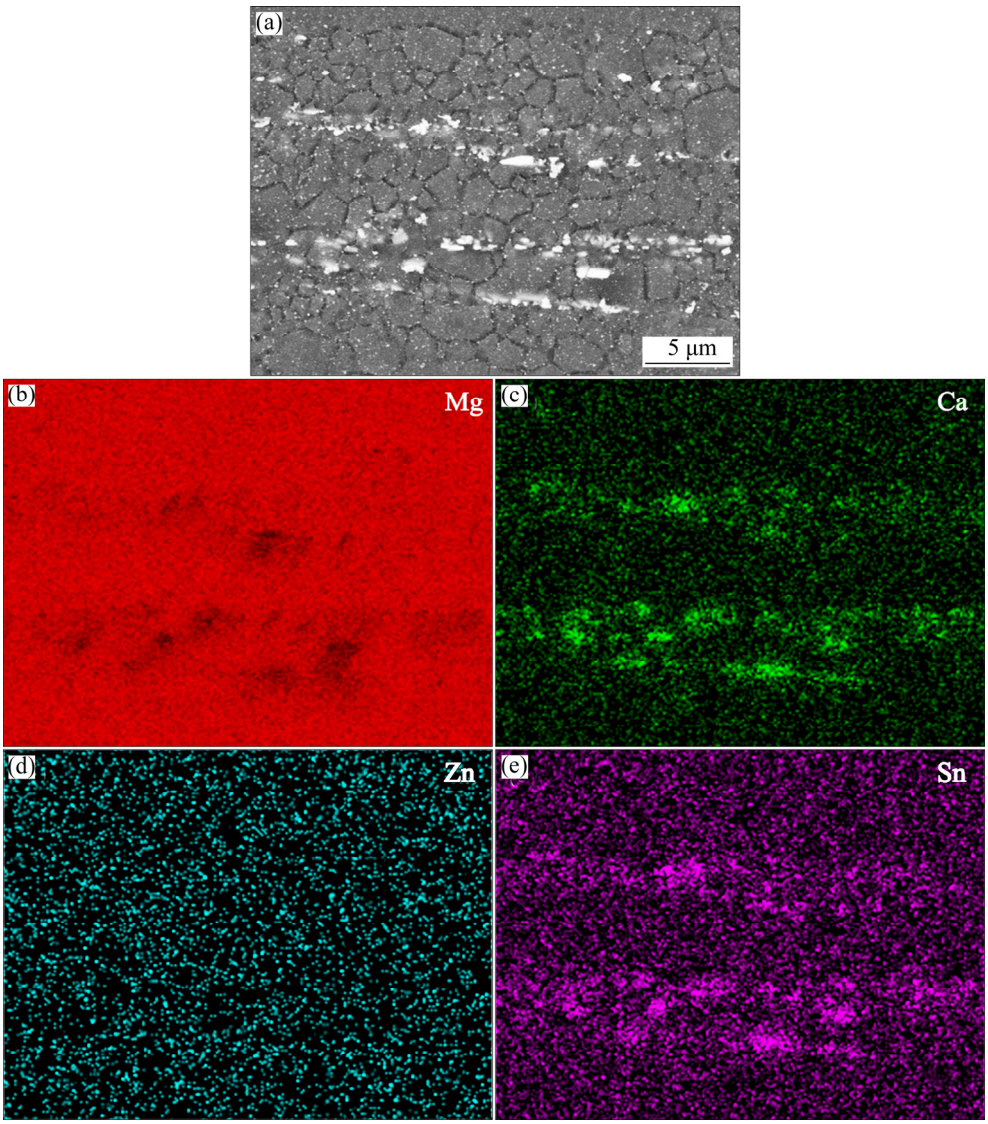

Fig. 5 Image mapping results of Mg, Sn, Zn and Ca elements in as-extruded TZX621 alloy with extrusion ratio of 16: (a) SEM image; (b) Distribution of Mg element; (c) Distribution of Ca element; (d) Distribution of Zn element; (e) Distribution of Sn element

extrusion ratio of 16 decreased obviously. According to EBSD statistics result, the average size of DRXed grains in as-extruded TZX621 alloy decreased from 2.16 to 1.57 mm. The difference in size of DRXed grains was attributed to the change of extrusion ratio. As mentioned above, due to the existence of CaMgSn phase, PSN mechanism played an important role in recrystallization of as-extruded TZX621 alloy. However, as seen in Fig. 4, the distribution of broken CaMgSn particles was inhomogeneous. In as-extruded TZX621 alloy with extrusion ratio of 6, due to its low extrusion ratio, complete DRX could only take place in regions where CaMgSn phase was enriched, and led to the formation of regions with fine DRXed grains. For the regions where the amount of CaMgSn phase was low, the activation of DRX was difficult. In as-extruded TZX621 alloy with extrusion ratio of 16, although the distribution of broken CaMgSn particles was also inhomogeneous, extrusion ratio as high as 16 ensured the high fraction of DRXed regions and also contributed to the decreased average size of DRXed grains.

Figure 7 shows the pole figures of as-extruded TZX621 alloy with different extrusion ratios. As seen in Fig. 7, as-extruded TZX621 alloy exhibited a type of basal fiber texture which was typical of Mg alloys, in which the {0001} plane was preferentially orientated parallel to the extrusion direction [18]. As the extrusion ratio was increased from 6 to 16, the basal texture was weakened and the maximum intensity decreased from 22.34 to 11.58. It was found in extruded Mg−Zn−Ca alloy that, increase of extrusion ratio from 10 to 20 also led to a significant decrease of basal texture intensity [19]. However, in as-extruded Mg−9Gd−4Y−0.4Zr alloy, a common extrusion texture was found at the low extrusion ratio of 8 while an unusual extrusion texture with the basal planes perpendicular to the extrusion

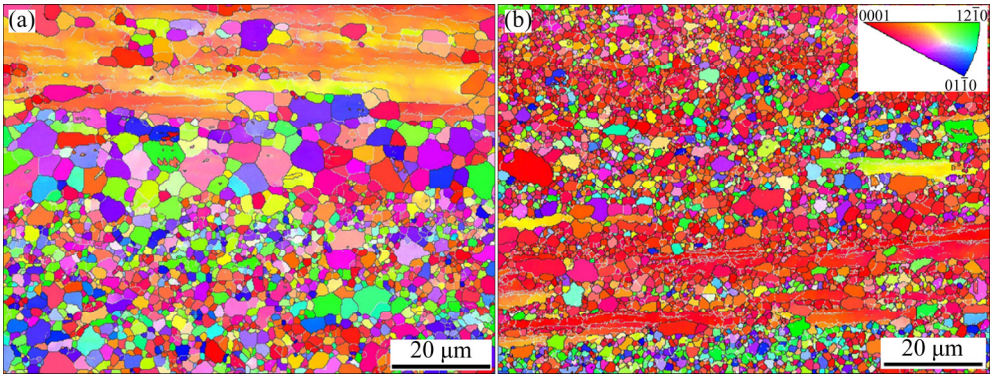

Fig. 6 Orientation maps of as-extruded TZX621 alloy with different extrusion ratios parallel to extrusion direction obtained by EBSD: (a) Extrusion ratio of 6; (b) Extrusion ratio of 16

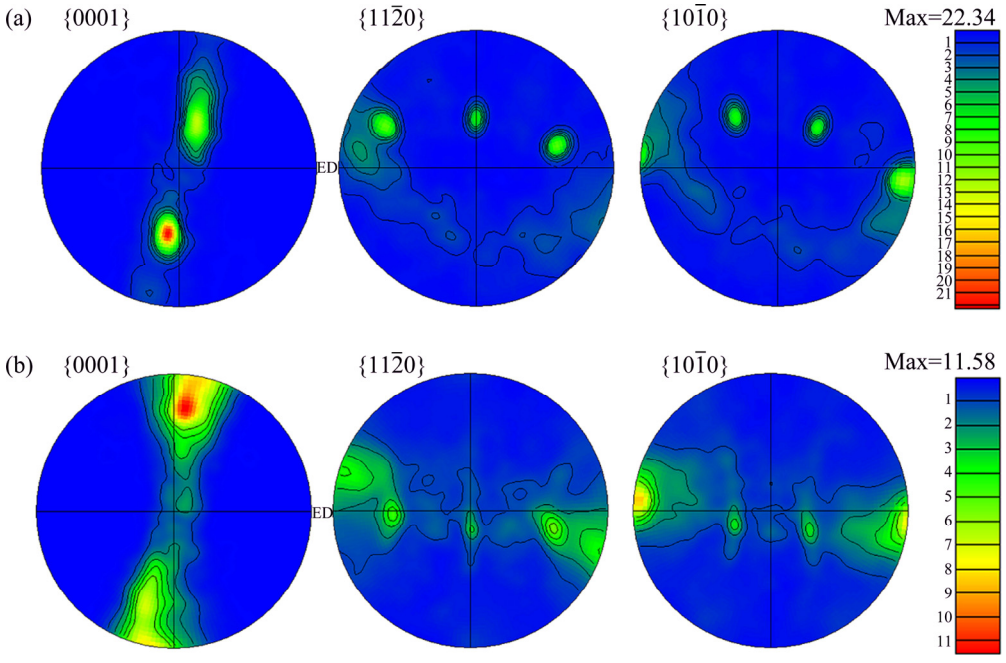

Fig. 7 Pole figures of as-extruded TZX621 alloy with different extrusion ratios obtained by EBSD: (a) Extrusion ratio of 6; (b) Extrusion ratio of 16

direction was observed at the high extrusion ratio of 19. It was concluded that the high extrusion ratio enabled the complete DRX and the modification in texture caused by RE addition was finished [20]. In extruded Mg alloys without RE, DRXed grains always presented a dispersive basal texture and coarse un-DRXed grains always exhibited strong basal texture. Therefore, the intensity of basal texture was related to un-DRXed grains to a great extent. In this work, both OM and EBSD analysis confirmed that, the increase of extrusion ratio from 6 to 16 led to a significant decrease of fraction of un-DRXed grains. The increase of extrusion ratio promoted DRX process and weakened the texture intensity simultaneously.

Figure 8 shows the misorientation angle distribution of as-extruded TZX621 alloy with different extrusion ratios. As shown in Figs. 8(a, b), the distribution of misorientation angles of as-extruded TZX621 alloy was different from ideal HCP structure, which indicated the formation of texture during hot extrusion. The difference in the distribution of misorientation angles between as-extruded TZX621 alloy with extrusion ratio of 6 and 16 was not obvious. However, the fraction of LAGBs in as-extruded TZX621 alloy with extrusion ratio of 16 was lower than that of as-extruded TZX621 alloy with extrusion ratio of 6. The reduction of fraction of LAGBs also confirmed a higher proportion of DRXed grains in as-extruded TZX621 alloy with extrusion ratio of 16.

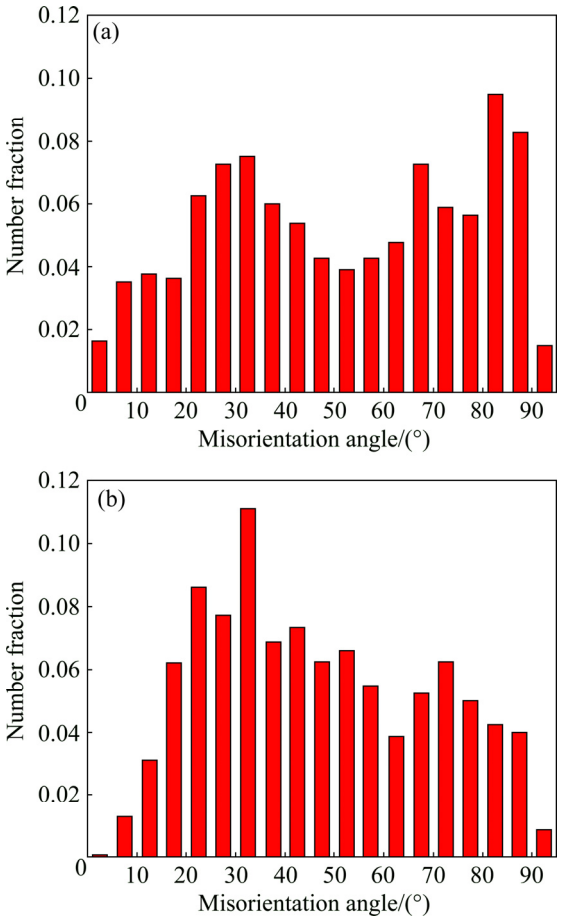

Fig. 8 Misorientation angle distribution of as-extruded TZX621 alloy with different extrusion ratios obtained by EBSD: (a) Extrusion ratio of 6; (b) Extrusion ratio of 16

Figure 9 shows the effect of extrusion ratio on mechanical properties of as-extruded TZX621 alloy and the specific data are summarized in Table 1. Yield strength (YS), ultimate tensile strength (UTS) and elongation to failure (E_f) of as-extruded TZX621 alloy with extrusion ratio of 6 were 166.8 MPa, 251.2 MPa and 15.6%, respectively. When the extrusion ratio was increased to 16, the mechanical properties of as-extruded TZX621 alloy were improved simultaneously. YS, UTS and E_f of as-extruded TZX621 alloy with extrusion ratio of 16 reached 226.9 MPa, 295.6 MPa and 18.1%, improved by 36.0%, 17.7% and 13.5%, respectively.

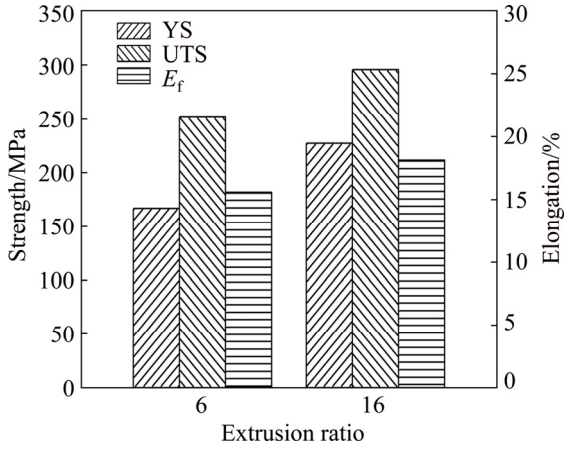

Fig. 9 Effect of extrusion ratio on mechanical properties of as-extruded TZX621 alloy

Table 1 Mechanical properties of as-extruded TZX621 alloy with different extrusion ratios

Extrusion ratio	YS/MPa	UTS/MPa	E_f/%
6	166.8	251.2	15.6
16	226.9	295.6	18.1

As seen in Fig. 9 and Table 1, YS of as-extruded TZX621 alloy was improved significantly when extrusion ratio was increased from 6 to 16. YS of wrought alloys usually comes from the strengthening effect of grain refinement, texture, solid solution and second phases [21]. In TZX621 alloy, since the solid solubility of Ca element in α-Mg matrix was low, Sn and Zn elements were the main solid solution elements. Especially, no Zn-contained phase was found in as-cast, as-homogenized nor as-extruded state. Therefore, most of Zn element was in α-Mg matrix and contributed to solid solution strengthening. Zn atoms dissolved in α-Mg matrix are effective in increasing the critical resolved shear stress of the basal slip system of Mg at room

temperature [22]. Sn atoms in as-extruded TZX621 alloy existed in three forms: (1) solute Sn atoms in α-Mg matrix, which also contributed to solid solution strengthening, (2) Sn atoms in CaMgSn phase and 3) in precipitated Mg_2Sn phase. Both broken CaMgSn phase and fine precipitated Mg_2Sn phase could act as barriers to dislocation motion and grain boundary sliding. The strengthening effect of Mg_2Sn phase precipitated in α-Mg matrix was more obvious than broken CaMgSn phase according to Orowan dislocation bypassing mechanism [23]. In this work, since TZX621 alloy ingot was subjected to the same homogenization treatment, the solid solution strengthening effect for as-extruded TZX621 alloy with different extrusion ratios was almost the same. Similarly, as seen in Fig. 4, change of extrusion ratio had little influence on size and distribution of broken CaMgSn phase and fine precipitated Mg_2Sn phase. Texture is also an important strengthening mechanism during the deformation of extruded Mg alloys. The basal slip is the dominant deformation system during the tensile deformation of extruded Mg alloy along the extrusion direction. The strong basal fiber texture formed in extruded Mg alloys can decrease the Schmid factor for the basal slip system and lead to an increase of YS [24]. Therefore, if only texture was taken into consideration, as-extruded TZX621 alloy with extrusion ratio of 6 should exhibit higher YS than that with extrusion ratio of 16. However, YS of as-extruded TZX621 alloy with extrusion ratio of 16 was 36.0% higher than that with extrusion ratio of 6. This phenomenon indicated that, the strengthening effect of texture was counteracted by other mechanism. As shown in Fig. 3 and Fig. 6, the increase of extrusion ratio from 6 to 16 led to a significant reduction in fraction of un-DRXed grains, which also led to a significant reduction in average grain size. According to Hall−Petch equation, the contribution of grain size to YS of a given alloy is proportional to $d^{-1/2}$. For Mg alloys with HCP structure, the strengthening effect of grain refinement is more significant than conventional steel and aluminum alloys. Therefore, the improvement in YS of as-extruded TZX621 alloy with increasing extrusion ratio was attributed to the increased DRX fraction and decreased size of DRXed grains.

The UTS of as-extruded TZX621 alloy was closely related to its work hardening ability, as well as its YS. According to the tensile test results, although both YS and UTS of as-extruded TZX621 alloy with extrusion ratio of 16 were higher than those of sample with extrusion ratio of 6, the improvement in UTS was lower than YS. These results indicated that the increase of extrusion weakened the work hardening ability of as-extruded TZX621 alloy. It is well known that grain refinement is the only way to improve the strength and elongation of metallic materials simultaneously. In this work, besides the improvement in YS and UTS, the further increase of E_f was also attributed to the grain refinement in as-extruded TZX621 alloy with the increase of extrusion ratio. Moreover, the relatively homogeneous microstructure in as-extruded TZX621 alloy with extrusion ratio of 16 could sustain larger deformation degree than that with extrusion ratio of 6.

4 Conclusions

1) As-cast TZX621 alloy consisted of α-Mg, Mg_2Sn and CaMgSn phases. After homogenization treatment, Mg_2Sn phase dissolved into α-Mg matrix while CaMgSn phase with high melting point remained.

2) Incomplete DRX took place in as-extruded TZX621 alloy during hot extrusion. As the extrusion ratio was increased from 6 to 16, the fraction of un-DRXed grains decreased from 31.3% to 13.2%. Coarse CaMgSn phase was broken into particles and distributed along the extrusion direction and the average size of DRXed grains in as-extruded TZX621 alloy decreased from 2.16 to 1.67 mm. Fine Mg_2Sn particles precipitated from α-Mg matrix during hot extrusion. As-extruded TZX621 alloy exhibited a type of basal fiber texture. As the extrusion ratio was increased from 6 to 16, the basal texture was weakened and the fraction of LAGBs was also reduced.

3) When the extrusion ratio was increased from 6 to 16, mechanical properties of as-extruded TZX621 alloy were improved comprehensively. YS, UTS and E_f of as-extruded TZX621 alloy with extrusion ratio of 16 reached 226.9 MPa, 295.6 MPa and 18.1%, which were improved by 36.0%, 17.7% and 13.5%, respectively, compared to those of as-extruded TZX621 alloy with extrusion ratio of 6. A significant reduction in fraction of un-DRXed grains and corresponding decrease of average grain size are the main reasons for the improvement in comprehensive mechanical properties of as-extruded TZX621 alloy.

References

[1] ZHANG Yao-cheng, YANG Li, DAI Jun, GE Jin-guo, GUO Guo-lin, LIU Zhong. Effect of Ca and Sr on the compressive creep behavior of Mg−4Al−RE based magnesium alloys [J]. Materials & Design, 2014, 63: 439−445.

[2] HUANG Zheng-hua, QI Wen-jun, XU Jing, CAI Chang. Microstructures and mechanical properties of Mg−Al−Sm series heat-resistant magnesium alloys [J]. Transactions of Nonferrous Metals Society of China, 2015, 25: 22−29.

[3] JIN Zhao-yang, LI Nan-nan, ZHANG Qi, YAN Kai, CUI Zhen-shan. Effects of forging parameters on uniformity in deformation and microstructure of AZ31B straight spur gear [J]. Transactions of Nonferrous Metals Society of China, 2017, 27: 2172−2180.

[4] WU Luo-yi, LI Hao-tian, YANG Zhong. Microstructure evolution

during heat treatment of Mg−Gd−Y−Zn−Zr alloy and its low-cycle fatigue behavior at 573 K [J]. Transactions of Nonferrous Metals Society of China, 2017, 27: 1026−1035.

[5] ZHANG Yu, WU Yu-juan, PENG Li-ming, FU Peng-huai, HUANG Fei, DING Wen-jiang. Microstructure evolution and mechanical properties of an ultra-high strength casting Mg−15.6Gd−1.8Ag−0.4Zr alloy [J]. Journal of Alloys and Compounds, 2014, 615: 703−711.

[6] LI Wan-dong, HUANG Xue-fei, HUANG Wei-gang. Effects of Ca, Ag addition on the microstructure and age-hardening behavior of a Mg−7Sn (wt%) alloy [J]. Materials Science and Engineering A, 2017, 692: 75−80.

[7] LUO Dan, WANG Hui-yuan, CHEN Lei, LIU Guo-jun, WANG Jin-guo, JIANG Qi-chuan. Strong strain hardening ability in an as-cast Mg−3Sn−1Zn alloy [J]. Materials Letters, 2013, 94: 51−54.

[8] LIU Chao-qiang, CHEN Hou-wen, NIE Jian-feng. Interphase boundary segregation of Zn in Mg−Sn−Zn alloys [J]. Scripta Materialia, 2016, 123: 5−8.

[9] TANG W N, PARK S S, YOU B S. Effect of the Zn content on the microstructure and mechanical properties of indirect-extruded Mg−5Sn−*x*Zn alloys [J]. Materials & Design, 2011, 32: 3537−3543.

[10] KHALILPOUR H, MIRESMAEILI S M, BAGHANI A. The microstructure and impression creep behavior of cast Mg−4Sn−4Ca alloy [J]. Materials Science and Engineering A, 2016, 652: 365−369.

[11] PARK S H, KIM S H, KIM H S, YOON J, YOU B S. High-speed indirect extrusion of Mg−Sn−Al−Zn alloy and its influence on microstructure and mechanical properties [J]. Journal of Alloys and Compounds, 2016, 667: 170−177.

[12] PAN Hu-cheng, QIN Gao-wu, XU Ming, FU He, REN Yu-ping, PAN Fu-sheng, GAO Zheng-yuan, ZHAO Chao-yong, YANG Qing-shan, SHE Jia, SONG Bo. Enhancing mechanical properties of Mg−Sn alloys by combining addition of Ca and Zn [J]. Materials & Design, 2015, 83: 736−744.

[13] WANG Ya-xiao, ZHOU Ji-xue, WANG Jie, LUO Tian-jiao, YANG Yuan-sheng. Effect of Bi addition on microstructures and mechanical properties of AZ80 magnesium alloy [J]. Transactions of Nonferrous Metals Society of China, 2011, 21: 711−716.

[14] ZHANG Xiao-bo, YUAN Guang-yin, NIU Jia-lin, FU Peng-huai, DING Wen-jiang. Microstructure, mechanical properties, biocorrosion behavior, and cytotoxicity of as-extruded Mg−Nd−Zn−Zr alloy with different extrusion ratios [J]. Journal of the Mechanical Behavior of Biomedical Materials, 2012, 9: 153−162.

[15] CHANG L L, TANG H, GUO J. Strengthening effect of nano and micro-sized precipitates in the hot-extruded Mg−5Sn−3Zn alloys with Ca addition [J]. Journal of Alloys and Compounds, 2017, 703: 552−559.

[16] ROBSON J D, HENRY D T, DAVIS B. Particle effects on recrystallization in magnesium–manganese alloys: Particle-stimulated nucleation [J]. Acta Materialia, 2009, 57: 2739−2747.

[17] YAN Bang-song, DONG Xuan-pu, MA Rong, CHEN Shu-qun, PAN Zhang, LING Hong-jiang. Effects of heat treatment on microstructure, mechanical properties and damping capacity of Mg−Zn−Y−Zr alloy [J]. Materials Science and Engineering A, 2014, 594: 168−177.

[18] HU Guang-shan, ZHANG Ding-fei, DONG Yu-feng, CHEN Xia, JIANG Lu-yao, PAN Fu-sheng. Microstructures and mechanical properties of as-extruded and heat treated Mg−6Zn−1Mn−4Sn−1.5Nd alloy [J]. Transactions of Nonferrous Metals Society of China, 2015, 25: 1439−1445.

[19] TONG L B, ZHENG M Y, CHENG L R, KAMADO S, ZHANG H J. Effect of extrusion ratio on microstructure, texture and mechanical properties of indirectly extruded Mg−Zn−Ca alloy [J]. Materials Science and Engineering A, 2013, 569: 48−53.

[20] ALIZADEH R, MAHMUDI R, NGAN A H W, LANGDON T G. An unusual extrusion texture in Mg−Gd−Y−Zr alloys[J]. Advanced Engineering Materials, 2016, 18: 1044−1049.

[21] WANG H Y, RONG Jian, LIU Guo-jun, ZHA Min, WANG Cheng, LUO Dan, JIANG Qi-chuan. Effects of Zn on the microstructure and tensile properties of as-extruded Mg−8Al−2Sn alloy [J]. Materials Science and Engineering A, 2017, 698: 249−255.

[22] WU K C, YEH J W, CHANG S Y. Refined microstructure and improved mechanical properties of high-ratio extruded AZ91−*x*Sn magnesium alloy [J]. Materials Chemistry and Physics, 2015, 162: 757−763.

[23] YANG Qiang, BU Fan-qiang, QIU Xin, LI Yang-de, LI Wei-rong, SUN Wei, LIU Xiao-juan, MENG Jian. Strengthening effect of nano-scale precipitates in a die-cast Mg−4Al−5.6Sm−0.3Mn alloy [J]. Journal of Alloys and Compounds, 2016, 665: 240−250.

[24] TANG W N, CHEN R S, ZHOU J, HAN E H. Effects of ECAE temperature and billet orientation on the microstructure, texture evolution and mechanical properties of a Mg−Zn−Y−Zr alloy [J]. Materials Science and Engineering A, 2009, 499: 404−410.

不同挤压比 Mg–Sn–Zn–Ca 合金的显微组织和力学性能

张 扬[1]，陈晓阳[2]，卢雅琳[1]，李小平[1]

1. 江苏理工学院 材料工程学院，常州 213001；2. 江苏理工学院 机械工程学院，常州 213001

摘 要：研究挤压比对 Mg−6Sn−2Zn−1Ca (TZX621，质量分数，%)合金显微组织和力学性能的影响。结果发现，挤压态 TZX621 合金中发生不完全再结晶；当挤压比从 6 增大至 16，未再结晶晶粒的相对含量和再结晶晶粒的平均尺寸均降低，基面织构强度也随之弱化。热挤压过程中，粗大 CaMgSn 相发生破碎，细小 Mg_2Sn 相则在 α-Mg 基体中析出。挤压比为 16 时，合金的屈服强度、抗拉强度和伸长率达到 226.9 MPa、295.6 MPa 和 18.1%，与挤压比为 6 时相比分别提高了 36.0%、17.7%和 13.5%。

关键词：镁锡合金；挤压比；显微组织；织构；力学性能

(Edited by Bing YANG)